# 1 A 0.5-million-year North African humid period preceded the

# 2 mid-Pliocene glaciation

- 3 Udara Amarathunga<sup>1,2</sup>, Eelco J. Rohling<sup>1,3</sup>, Katharine M. Grant<sup>1</sup>, Alexander Francke<sup>4</sup>, James
- 4 Latimer<sup>5</sup>, Robert M. Klaebe<sup>4</sup>, David Heslop<sup>1</sup>, Andrew P. Roberts<sup>1</sup>, David K. Hutchinson<sup>6</sup>.
- <sup>1</sup>Research School of Earth Sciences, Australian National University, ACT 2601, Canberra,
- 6 Australia.
- <sup>2</sup>Department of Geosciences, Guyot Hall, Princeton University, Princeton NJ 08544
- 8 <sup>3</sup>Ocean and Earth Science, University of Southampton, National Oceanography Centre,
- 9 Southampton, UK.
- 10 <sup>4</sup>School of Physics, Chemistry and Earth Sciences, Faculty of Sciences, Engineering and
- 11 Technology, The University of Adelaide, 5005 Adelaide, South Australia, Australia
- <sup>5</sup>Fenner School of Environment and Society, Australian National University, ACT 2601,
- 13 Canberra, Australia.
- <sup>6</sup>Climate Change Research Centre and Australian Centre for Excellence in Antarctic Science,
- 15 University of New South Wales, Sydney, Australia
- Past North African humid periods resulted in expanded vegetation over the Sahara, due
- 17 to northward tropical African rainbelt displacement, opening new migration pathways
- 18 for hominins<sup>1-4</sup>. Commonly, these precession-timed North African humid periods ended
- within 15 thousand years due to rainbelt retreat<sup>5,6</sup>. Eastern Mediterranean organic-rich
- 20 layers (sapropels) reflect North African humid periods, at least back to 8 Myr<sup>ref.4</sup>. Here
- 21 we combine climate modelling with new and published proxy data to show that weakened
- sapropel preservation during the warm 5.3-3.3 Myr period<sup>7,8</sup> resulted from nutrient
- 23 runoff limitation associated with enhanced North African vegetation cover due to a
- 24 persistently more northward-located African monsoon front, relative to the mid-Pliocene
- 25 (3.3-3.0 Myr, when glacial intensity increased). We find that sapropel absence between
- 3.8 and 3.3 Myr coincided with maximum long-term monsoon flooding and landscape
- 27 stabilization by extension of humid, vegetated conditions throughout North Africa. Our
- 28 model results indicate that this 0.5-Myr-long Pan-North African humid period (Pan-
- 29 NAHP) ended at ~3.3 Myr because of southward African monsoon front displacement
- 30 with the initiation of major Northern Hemisphere glaciations. The 3.8-3.3 Myr Pan-
- 31 NAHP coincided with the earliest known evidence for hominin coexistence over Eastern
- and Central North Africa9. We posit that persistent green corridors during the Pan-
- NAHP facilitated connectivity and migration of early hominins, expanding their habitat
- 34 range over the wider North African territory.

#### Main

36

- North Africa (the present-day Sahara) has experienced astronomical precession controlled wet-
- dry cycles for at least the past 11 million years (Myr)<sup>10</sup>. The wet episodes, known as Green
- 39 Sahara Periods (GSPs) or African Humid Periods (AHPs), resulted from northward migration
- of the tropical African rainbelt during periods of increased boreal summer insolation<sup>2,11</sup>.
- 41 Periodic occurrence of AHPs modified North African hydrology, leading to establishment of
- 42 vast fluvial systems consisting of interconnected lakes, rivers, and inland deltas<sup>2,12</sup>.
- Consequently, savannah vegetation expanded over much of the currently hyper-arid landscape
- north of the Sahel<sup>4,5</sup>. Expanded vegetation led to development of 'green corridors', which
- enabled migration of hominins and other animals northward of the Sahel, into the otherwise
- inhospitable desert landscape<sup>3,4</sup>. AHPs typically terminated within a period of 8-15 thousand
- 47 years as the African rainbelt retreated equatorward, progressively re-establishing hyper-arid
- 48 conditions over the Sahara $^{1,4-6}$ .
- 49 More recent AHPs (notably, the last AHP; 14.8-5.5 thousand years ago) have been studied
- 50 using both terrestrial and marine geological records<sup>2,5,12</sup>. However, onshore fossil and
- environmental evidence of AHPs is increasingly rare going back through time<sup>4</sup>. Occurrence of
- 52 AHPs through the past few million years is best documented offshore in the eastern
- Mediterranean sedimentary record, in the form of organic-rich layers known as sapropels<sup>2,4</sup>.
- Thus, the presence of Mediterranean sapropels is an important tracer of past AHPs back to the
- 55 Late Miocene, which enables identification of over 230 humid episodes during the past ~8
- 56 Myrs<sup>4</sup>.

65

- 57 A 5.3-Myr eastern Mediterranean sapropel compilation indicates a phase of infrequent,
- irregular sapropel deposition from 5.3 to 3.3 Myr, with an absence of preserved sapropels
- 59 between 3.7 and 3.3 Myr. This Early Pliocene phase of sporadic sapropel preservation
- terminated with initiation of Northern Hemispheric (NH) glacials at ~3.3 Myr (Fig. 1, Fig. 2,
- Extended Data Fig. 1). Here we investigate the nature and termination of this interval using
- 62 new and compiled environmental proxy data that we interpret with targeted climate modelling
- scenarios. We then consider potential wider implications with respect to African landscape
- development, initiation of major northern hemisphere glaciation, and hominin evolution.

#### Eastern Mediterranean sapropel record

- 66 Sapropel formation during AHPs was driven by enhanced monsoon runoff to the
- 67 Mediterranean via the Nile River and along the wider North African margin, during NH

insolation maxima (precession minima)<sup>13,14</sup>. Strong evidence for enhanced freshwater flux within sapropels is imprinted as distinct negative anomalies in stable oxygen isotope ( $\delta^{18}O_{Calcite}$ ) measurements of surface-dwelling (planktonic) foraminiferal calcium carbonate shells<sup>14,15</sup>. Enhanced monsoon runoff supplied nutrients that increased primary productivity, and curtailed deep water ventilation due to surface-water buoyancy increase, which together led to preservation of sinking organic matter<sup>14,16</sup>. However, not every precession minimum resulted in sapropel formation<sup>14</sup>. Instead, sapropels commonly formed as clusters during intervals of high-amplitude precession minima<sup>14</sup>, related to orbital eccentricity maxima.

Eastern Mediterranean Ocean Drilling Program (ODP) sites provide a sapropel record back to the Miocene/Pliocene boundary<sup>7,8,17</sup>. Here we compile the main deep basin sediment records (ODP sites 964, 966, 967, 969) to generate a stack of preserved sapropels through the past 5.3 Myr (Fig. 1, Extended Data Fig. 1). We observe that sapropels are significantly less frequently preserved before 3.3 Myr, than afterwards. This pattern corroborates a suggestion based on ODP Site 967 geochemical records alone<sup>7</sup> (Fig. 1, Extended Data Fig. 1) that, after 3.2 Myr, an increase in the North African arid:humid contrast between AHPs and intervening dry intervals within each precession cycle gave rise to a more erodible landscape during arid periods<sup>7</sup>. Past and modern erodibility reconstructions have shown that dry, barren landscapes during glacial periods (which caused arid conditions over North Africa) led to higher erosion rates, which subsequently reduced during lengthy humid intervals when the landscape stabilized due to increased vegetation cover<sup>18</sup>. Therefore, higher erosion rates during dry intervals after 3.2 Myr would have resulted from minimized vegetation cover, leading to landscape instability and an increase in nutrient release via runoff. Increased nutrient discharge into the Mediterranean by monsoon runoff during subsequent humid intervals then resulted in enhanced productivity and, thus, increased organic carbon burial, as reflected from a rapid increase in Ba/Al ratio<sup>7</sup> (Fig. 1). However, no mechanism was established to explain the inferred aridity increase during North African dry periods after ~3.2 Myr.

# Climate modelling results: termination of Early Pliocene humid conditions

We find that eastern Mediterranean organic carbon burial intensification at 3.2 Myr followed initiation of NH glaciation across the 3.4-3.2 Myr interval (M2 glaciation at ~3.3 Myr)<sup>19</sup>. We observe increased mid-Pliocene (3.3-3.0 Myr) glacial ice volumes relative to the Early Pliocene, following a rapid ice volume increase during the M2 glaciation<sup>19</sup> (Fig. 1, Extended Data Fig. 2). We hypothesize that the North African landscape changes that led to the observed

change in sapropel preservation around 3.3 Myr may have resulted from NH glacial intensification. To explore North African landscape/climate evolution before and after the M2 glaciation, we perform climate model simulations focussed on contrasting ice volumes (based on published ice volume reconstructions<sup>19</sup>) during the Early Pliocene (5.3-3.4 Myr), the M2 glaciation, and subsequent mid-Pliocene glacials (Methods, Extended Data Table 1).

100

101

102

103

104

105

106

107

108

109

110

111

112

113

114

115

116

117

118

119

120

121

122

123

124

125

126

127

128

129

130

131

Polar ice sheet growth strengthens lower atmospheric meridional temperature gradients, resulting in more vigorous meridional atmospheric circulation cells, and changing precipitation patterns<sup>20,21</sup>. Accordingly, our climate model results indicate that NH meridional atmospheric circulation strengthened considerably, as polar ice sheets expanded during the M2 glaciation (Fig. 2, Methods). Over North Africa, stronger meridional circulation manifests during boreal summer in intensification of subsidence over the Mediterranean, and ascent over the Sahel. Importantly, we observe a 2°-3° southward shift of the 850 hPa easterly-westerly wind convergence zone over North Africa, which implies a southward displacement of the African monsoon front due to NH polar cooling<sup>21,22</sup> (Extended Data Fig. 3). Our interpretation is supported by a notable decrease of 600 hPa ascent at ~20°N beyond the Sahel. Consequently, North African precipitation markedly decreases during the M2 glaciation, relative to the Early Pliocene (Fig. 2). Furthermore, we find that similar (albeit less intense) dry conditions occurred also during subsequent, less-intense mid-Pliocene glacials (Extended Data Fig. 4). We observe similar zonal wind and precipitation variability patterns, with less severity than during the M2 glacial. Thus, enhanced aridity and sediment erodibility during North African dry phases (insolation minima, which were largely contemporaneous to NH glacials) since 3.3 Myr may have increased runoff-driven nutrient discharge during subsequent humid phases, and thus favoured sapropel formation following enhanced organic carbon burial and subsequent preservation due to stratification-driven bottom anoxia. Conversely, more persistently humid conditions associated with reduced NH ice volumes before 3.3 Myr may have enhanced North African vegetation cover beyond the Sahel (due to more northerly monsoon front), thereby reducing erodibility during relatively arid phases, limiting the probability of sapropel preservation. We note that our model simulations use prescribed vegetation fields as boundary conditions, which are held fixed through all 3 simulations (Methods). Previous Pliocene simulations have shown that dynamic vegetation feedbacks can amplify changes made by CO<sub>2</sub> and ice sheet reductions<sup>23</sup> or orbital variations<sup>24</sup>. Since vegetation feedbacks are not included in our simulations but tend to force in the same direction of drying/wetting as the ice sheet forcing, we expect that the precipitation changes we have found may be even stronger if they were simulated in a model with dynamic vegetation (see Methods).

132

133

134

135

136

137

138

139

140

141

142

143

144

145

146

147

148

149

150

151

152

153

154

155

156

157

158

159

160

161

162

163

A notable shift to more positive long-term mean planktonic foraminiferal  $\delta^{18}$ O<sub>Calcite</sub> between 3.4 and 3.2 Myr at ODP Site 967 offers evidence for decreased long-term mean freshwater runoff to the Mediterranean. We observe generally more negative long-term mean  $\delta^{18}$ O values through the Early Pliocene (before 3.4 Myr) compared to the period afterward, which we confirm with statistical analyses. However, there is a clear long-term shift of ≥0.3 ‰ to even more negative  $\delta^{18}O_{Calcite}$  values at ~3.8 Myr, which lasted until the M2 glaciation (Fig. 3, Extended Data Fig. 2); the 3.8-3.3 Myr period contains the most negative long-term  $\delta^{18}O_{Calcite}$ values since the Miocene. We do not observe a corresponding global ice volume shift, which suggests that the 3.8-3.3 Myr low  $\delta^{18}O_{Calcite}$  values reflect a freshwater-borne anomaly for the Pliocene (i.e., Such a negative  $\delta^{18}O_{Calcite}$  anomaly can be caused by the freshwater amount and/or freshwater  $\delta^{18}$ O. In the next section, we use geochemical data to confirm an increase in terrestrial runoff to the eastern Mediterranean)<sup>15,25</sup> (Fig. 1, Fig. 3, Extended Data Fig. 2). While individual  $\delta^{18}$ O maxima (which indicate non-sapropel/arid intervals during precession maxima) reached similar values (~1‰) during the 5.0-3.8 Myr and 3.3-3.0 Myr intervals, even individual  $\delta^{18}$ O maxima were more negative ( $\sim 0$  %) within the 3.8-3.3 Myr interval. To estimate a possible range of mean freshwater runoff increase that could have generated the observed  $\geq 0.3$  % shift to negative  $\delta^{18}$ O at 3.8 Myr, we employed a Mediterranean box model (Methods). Our sensitivity tests indicate that an increase of up to 1.6 times the pre-Aswan Nile runoff can generate such a shift to generally more negative  $\delta^{18}$ O values (Extended Data Fig. 2).

# Observation-based Pan-North African humid period

We find that the longest period of preserved sapropel absence extends within the  $\sim$ 3.7-3.3 Myr interval (with only two sapropels with low organic carbon contents at 3.8-3.7 Myr), even though a high-amplitude precession cluster exists within this period centred at  $\sim$ 3.5 Myr, which should have led to enhanced productivity and sapropel preservation (Fig. 3, Methods). While sapropel absence is usually observed during low-amplitude precession clustered modulated by eccentricity minima<sup>14,26</sup> (hence, reduced insolation and monsoon strengths, for example 2.6-2.4 Myr, 1.0-0.8 Myr - see Extended Data Fig. 1), sapropel absence within a high-amplitude precession cluster is a clear anomaly within an otherwise predictable sapropel formation and preservation pattern in relation to insolation. Despite  $\delta^{18}$ O values being more negative across

the 3.8-3.3 Myr interval (indicative of elevated freshwater runoff), the absence of preserved 164 sapropels suggests even lower eastern Mediterranean productivity (lower nutrient runoff due 165 to further reduced North African erodibility) than during the rest of the Early Pliocene, leading 166 to complete post-depositional oxidation of any organic carbon that reached the sea floor. 167 Core-scanning X-ray fluorescence (XRF) data corroborate our interpretations of enhanced 168 freshwater runoff, and decreased erodibility over North Africa. In eastern Mediterranean 169 sediments, the Ti/Al ratio is an established indicator of relative aeolian versus fluvial input<sup>7,14</sup>. 170 Low long-term earliest Pliocene mean Ti/Al values gradually increase to a maximum at ~3.9 171 Myr, followed by an abrupt return to lower values at ~3.8 Myr (Fig. 3). This supports our 172 δ<sup>18</sup>O<sub>Calcite</sub> interpretation of a shift to higher relative fluvial input at ~3.8 Myr. Lower Ti/Al 173 values are then maintained until ~3.3 Myr (M2 glaciation), where values increase again 174 afterwards. Our data also indicate that the 3.9-3.8 Myr shift toward lower Ti/Al values occurred 175 during both the alternating humid (sapropel) and dry (marl) intervals (Extended Data Fig. 5b), 176 whereas the shift to higher Ti/Al values at ~3.3 Myr occurred mainly due to increasing aridity 177 in dry intervals (Extended Data Fig. 5). 178 The Nile River is the primary fluvial sediment source to the modern eastern Mediterranean<sup>27,28</sup>. 179 Sediment provenance analysis and end-member modelling of modern eastern Mediterranean 180 sediments indicate that most Nile River terrigenous input originates from the Ethiopian 181 Highlands in East Africa<sup>27–29</sup>. The major aeolian dust input into the eastern Mediterranean 182 originates from central Libya in North Africa<sup>30</sup>. Nd isotope data for eastern Mediterranean 183 sediment provenance indicate that terrigenous sediment sources were persistently in Northeast 184 and East Africa across sapropel-marl cycles of the past 110,000 years (εNd within -1 to -8)<sup>29</sup>. 185 To evaluate if eastern Mediterranean sediment source regions changed considerably through 186 the past 5 Myr, we present new Nd isotope values of the Site 967 sediment clay fraction (Fig. 187 3c). The εNd for sapropels ranges within a narrow window of -4.3 to -6.7, which implies little 188 provenance change through time. This range also agrees with that found in late Quaternary 189 sapropels (approximately -3 to -7)<sup>29</sup>, and likely represents sediments originating mainly from 190 the Blue Nile (Ethiopian Highlands)<sup>28</sup> (Fig. 3, Extended Data Fig. 6). Within intercalated marls, 191 εNd ranges between -4.0 and -8.4, where more negative values might indicate higher relative 192 Central Sahara (-10 to -15) or White Nile (ENd ~-10) contributions<sup>28,29,31</sup> (Fig. 3, Extended 193 Data Fig. 6). Thus, our data indicate that eastern Mediterranean terrigenous sediment sources 194 remained confined largely to North-entral and Northeast-East African regions through the past 195

5 Myr.

Off the coast of Northwest Africa, ODP Site 659 provides the longest available Saharan aridity and dust export record, which demonstrates astronomically paced northwestern Saharan humid-dry oscillations over the past 11 Myr<sup>10</sup>. ODP Site 659 is located underneath the main modern Sahara dust plume, where most of the aeolian input originates from the West and Central Sahara (North-West to North-Central Africa)<sup>10</sup> (Extended Data Fig. 6). For ODP Site 659, the [Al+Fe]/[Si+Ti+K] ratio was used as an indicator of relative fluvial versus aeolian sediment input from Northwest Africa (higher values indicate more humid conditions with more intense chemical weathering). Intriguingly, there is a shift to increased fluvial input in ODP Site 659 at ~3.8 Myr, similar to that observed here in ODP Site 967 geochemical records (Fig. 3d). The [Al+Fe]/[Si+Ti+K] ratio decreases rapidly at the M2 glaciation, which reflects termination of the enhanced humid conditions of the 3.8-3.3 Myr period (Fig. 3b, Extended Data Fig. 6). Moreover, our 2 lowest Pliocene «Nd values appear within the sapropel-barren interval, indicating likely increased terrigenous input from sustained central Saharan palaeoriver discharge during precession maxima (continuing humid conditions even during the relatively arid intervals), through the Northeast African margin to the Mediterranean (Fig. 3, Extended Data Fig. 5). Simultaneous emergence of enhanced humid conditions across Northwest, North-central and Northeast Africa implies the existence of a Pan-North African humid period (Pan-NAHP) between 3.8 and 3.3 Myr.

Our observation of enhanced humidity during the Pan-NAHP, relative to the entire Early Pliocene, is supported by additional East and Northcentral African geological records. East African rift system (EARS) lake clusters were coeval to eastern Mediterranean sapropel clusters during high amplitude precession minima<sup>4,32–34</sup> (Fig. 4). Notably, deep EARS lake clusters existed in the Turkana and Afar basins between 3.7 and 3.4 Myr, indicating substantially increased humidity<sup>33,34</sup> (Fig. 4b). Palaeoenvironmental reconstructions using fossil assemblages estimated ~doubled precipitation during deposition of the Lokochot member (3.6-3.4 Myr) of the Koobi Fora Formation, eastern Lake Turkana shores, relative to the Early Pliocene<sup>35</sup>. In agreement, past woody cover reconstructions using fossil soils reveal maximum woody cover in the Omo-Turkana Basin and Awash Valley (Afar Basin) for the past 6 Myr at 3.6-3.4 Myr, in agreement with lowered soil carbonate  $\delta^{13}$ C values covering the wider EARS<sup>36,37</sup> (Fig. 4c). Moreover, megalake Chad in North-central Africa is the dominant hydrological feature recognized during past AHPs<sup>4,38</sup>. Analysis of Chad basin environmental conditions using Be isotopes reveals Plio-Pleistocene lacustrine sediment deposition centred at ~2.31±0.21 Myr, 3.00±0.19 Myr, 3.60±0.13 Myr and 4.20±0.19 Myr<sup>38</sup>, with maximum

Pliocene sedimentation rates between 3.7 and 3.4 Myr, which has been attributed to enhanced runoff intensity under humid conditions<sup>39</sup> (Fig. 4b). In summary, North-central and East African lacustrine records indicate that the coevally wettest Pliocene phase of these regions occurred simultaneous to the Pan-NAHP identified here.

## Wider implications and possible influence on early hominin dispersal

Our climate model results indicate that generally humid conditions over North Africa before 3.3 Myr resulted from a persistently more northerly monsoon front, relative to the mid-Pliocene, which enhanced precipitation over the Sahara and Ethiopian Highlands (Fig. 4e). Our results support previous suggestions of globally coherent humid subtropics through the warm Early Pliocene, due to decreased global meridional temperature gradients<sup>40</sup>. Moreover, we find that the long-term North Atlantic meridional temperature gradient decreased stepwise since ~3.9 Myr, culminating in lowest values at 3.6-3.4 Myr. North Atlantic warmth is reflected by reduced NH ice volumes and elevated global sea levels during the Pan-NAHP<sup>41,42</sup> (Extended Data Fig. 7). We postulate that reduced meridional temperature gradients during the Pan-NAHP, compared to the rest of the Pliocene, may have optimized northward tropical African monsoon front displacement, yielding more humid conditions over North Africa<sup>11,43</sup>.

Finally, our findings provide new insights into environmental changes associated with African early hominin evolution and dispersal. Australopithecine remains have been recovered from multiple locations over East and Central Africa during the 3.7-3.3 Myr period (within the Pan-NAHP identified here) 44-46 (Fig. 4, Extended Data Fig. 8). While it has been suggested that hominin diversity expanded within this period, apparent diversity expansion might reflect improved sample availability relative to the rest of the Early Pliocene<sup>47</sup>. Australopithecus bahrelghazali from the Chad Basin (3.58±0.27 Myr, the oldest existing Pliocene hominin fossil remains from Central Africa)<sup>9,38</sup> was contemporaneous to the East African australopithecine remains recovered some ~2,500 km to the west from Turkana and Afar basins 44,48 (Fig. 4, Extended Data Fig. 8), although it remains ambiguous whether A. bahrelghazali was a geographical variant within the A. afarensis taxon, or a different species 45,46. Periods of enhanced humidity are associated with increasing hominin habitat suitability beyond the Sahel, and hydrological modelling demonstrates that the probability of along-rift hominin dispersal increases under more humid conditions<sup>49,50</sup>. Accordingly, it has been proposed that stable Pliocene climate periods (with major lake phases) provided vegetated corridors for early hominins to migrate out of east African refuge areas to the adjacent rift valleys and beyond<sup>34</sup>.

Our analysis here suggests that simultaneous major Central and East African Lake phases, together with maximum woody cover (reaching 60%) to the North of Turkana Basin<sup>36</sup>, occurred only during the Pan-NAHP (Fig. 4). While the source of hominin dispersal to Northcentral Africa is uncertain due to inadequate fossil records from Northwest and Northernmost Africa, we infer that the 3.8-3.3 Myr Pan-NAHP reconstructed here may have facilitated the earliest known expansion of hominin geographical range toward the Chad basin, likely via enduring green corridors connecting open East African habitats with North African Savannah<sup>34</sup> (Extended Data Fig. 8).

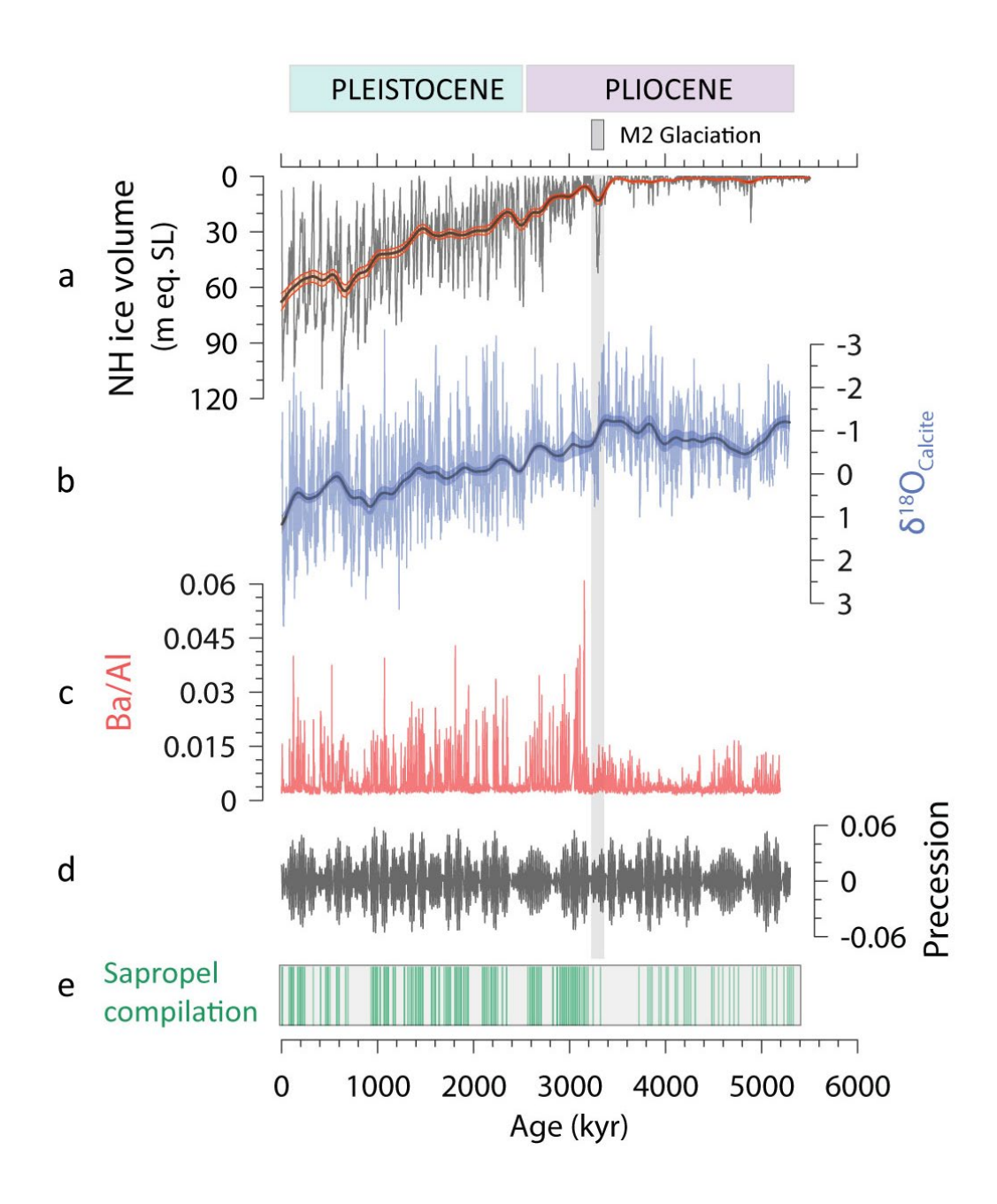


**Figure 1**| **Eastern Mediterranean sapropels across the past 5 Myr. a,** NH ice volume evolution through the Plio-Pleistocene<sup>19</sup>. A rapid ice volume increase during glaciation M2 (~3.3 Myr.) is indicated. Mean NH ice volume increases across the shaded transition (3.4-3.2 Myr) **b,** ODP Site 967 stable oxygen isotope record<sup>7</sup>. For **a** and **b**, thick black lines represent a 60-kyr moving average, where upper and lower lobes indicate 95% upper and lower confidence intervals. **c,** ODP Site 967 Ba/Al record, in which enhanced organic carbon burial is evident after 3.2 Myr<sup>7</sup>. **d,** Orbital precession variability through the Plio-Pleistocene<sup>26</sup>. **e,** Eastern Mediterranean sapropel stack (see Methods). Sapropel occurrence is sporadic between 5.3 and 3.3 Myr. No sapropels are preserved within the 3.7-3.3 Myr period, with only two low-organic carbon sapropels existing within the 3.8-3.72 Myr period.

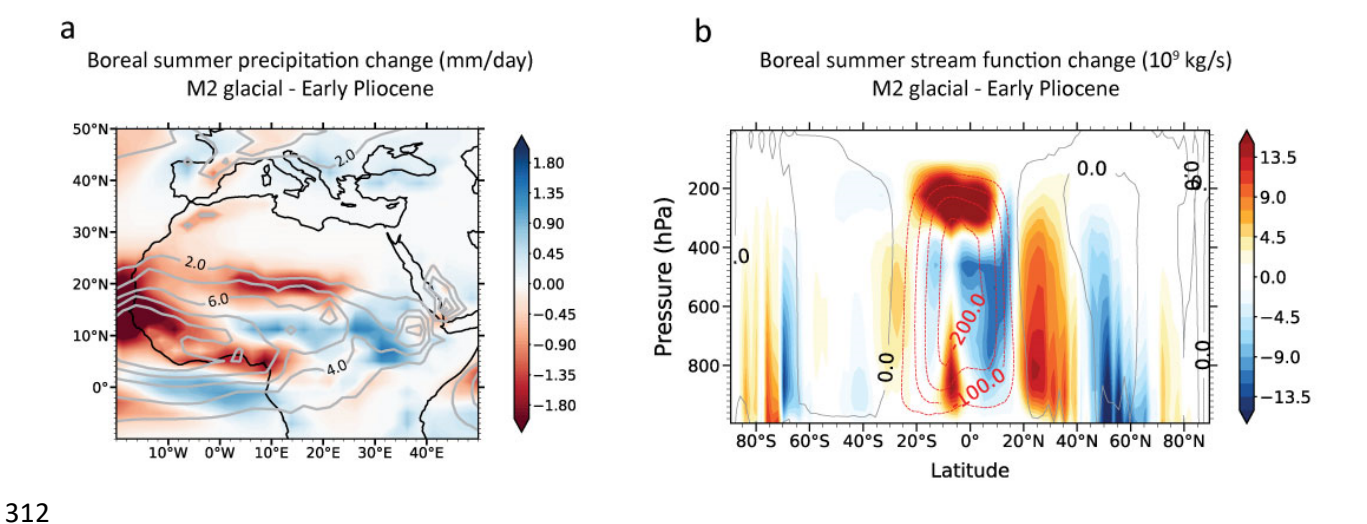
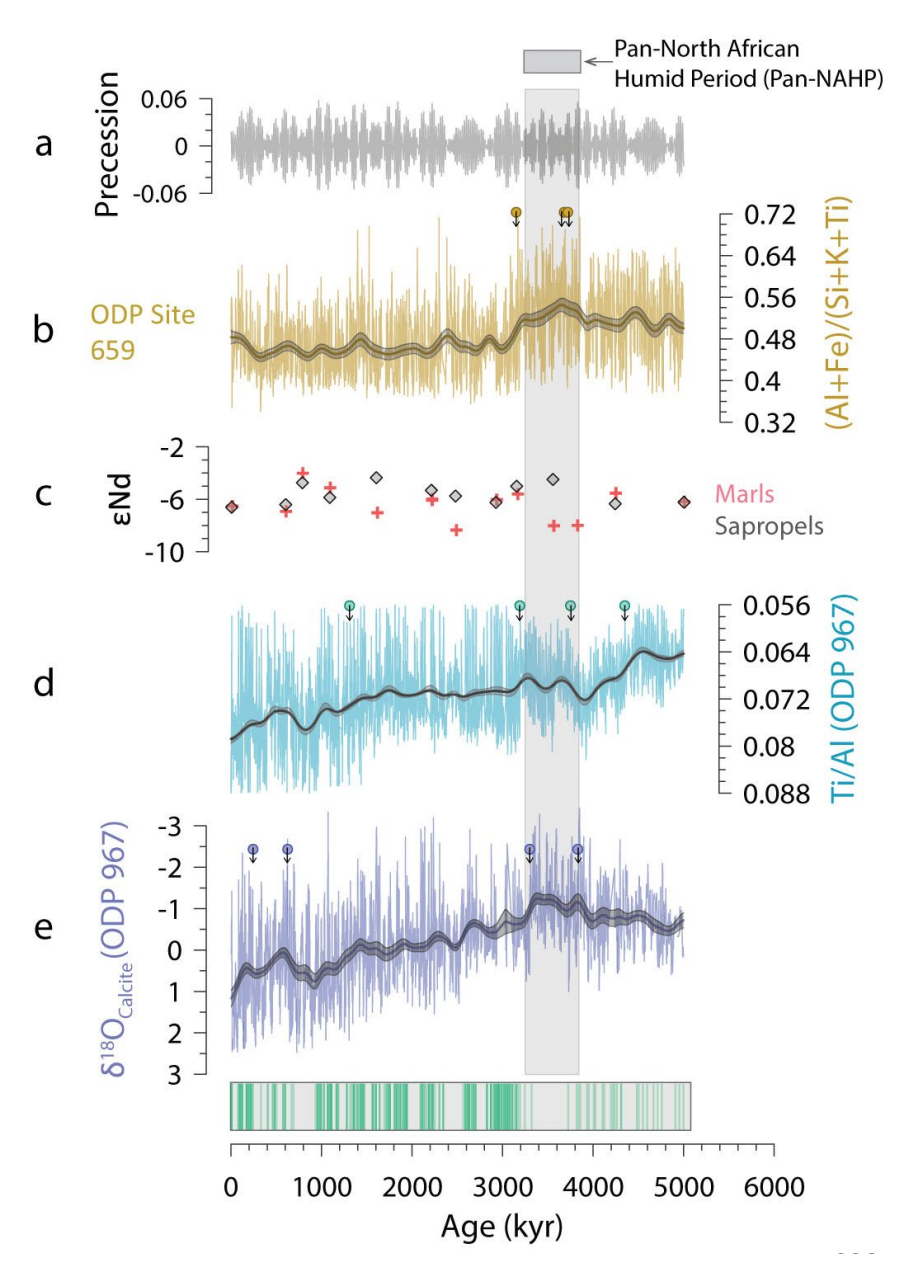


Figure 2| North Africa drying during the M2 glaciation. a, Boreal summer precipitation change (M2 glacial-Early Pliocene), with strong drying over North Africa. Contours indicate Early Pliocene isohyets. b, Zonal mean meridional stream function change for boreal summer. Contours represent Early Pliocene wind velocities. Positive (grey) contour values indicate clockwise overturning circulation; negative (red) contour values indicate anti-clockwise overturning circulation. The Southern Hemisphere Hadley cell strengthens and contracts (with a tropopause height decrease), while all NH meridional cells are strengthened during the boreal summer.



**Figure 3**| **Evidence for enhanced humid conditions across North Africa during the 3.3-3.8 Myr interval. a,** Orbital precession variability through the Plio-Pleistocene<sup>26</sup>. **b,** West African ODP Site 659 [Al+Fe]/[Si+K+Ti] ratio, where higher values indicate more fluvial sediment input under more humid conditions. **c,** ODP Site 967 ɛNd values for sapropel and marl sediments back to the Miocene-Pliocene boundary (see Extended Data Fig. 6 for provenance). **d,** Eastern Mediterranean ODP Site 967 Ti/Al ratio<sup>7</sup>, where lower values indicate more alluvial sediment input. **e,** ODP Site 967 stable oxygen isotope record, indicating considerably negative mean values across the Pan-NAHP (highlighted in grey). Coloured dots (marked with arrows) for b, d and e represent linear change points for each record (Methods). Eastern Mediterranean sapropel stack is shown above the age axis. More extreme individual data points for panels b and d are not shown. See Extended Data Fig. 5 panels b and d for complete range of data for each record.

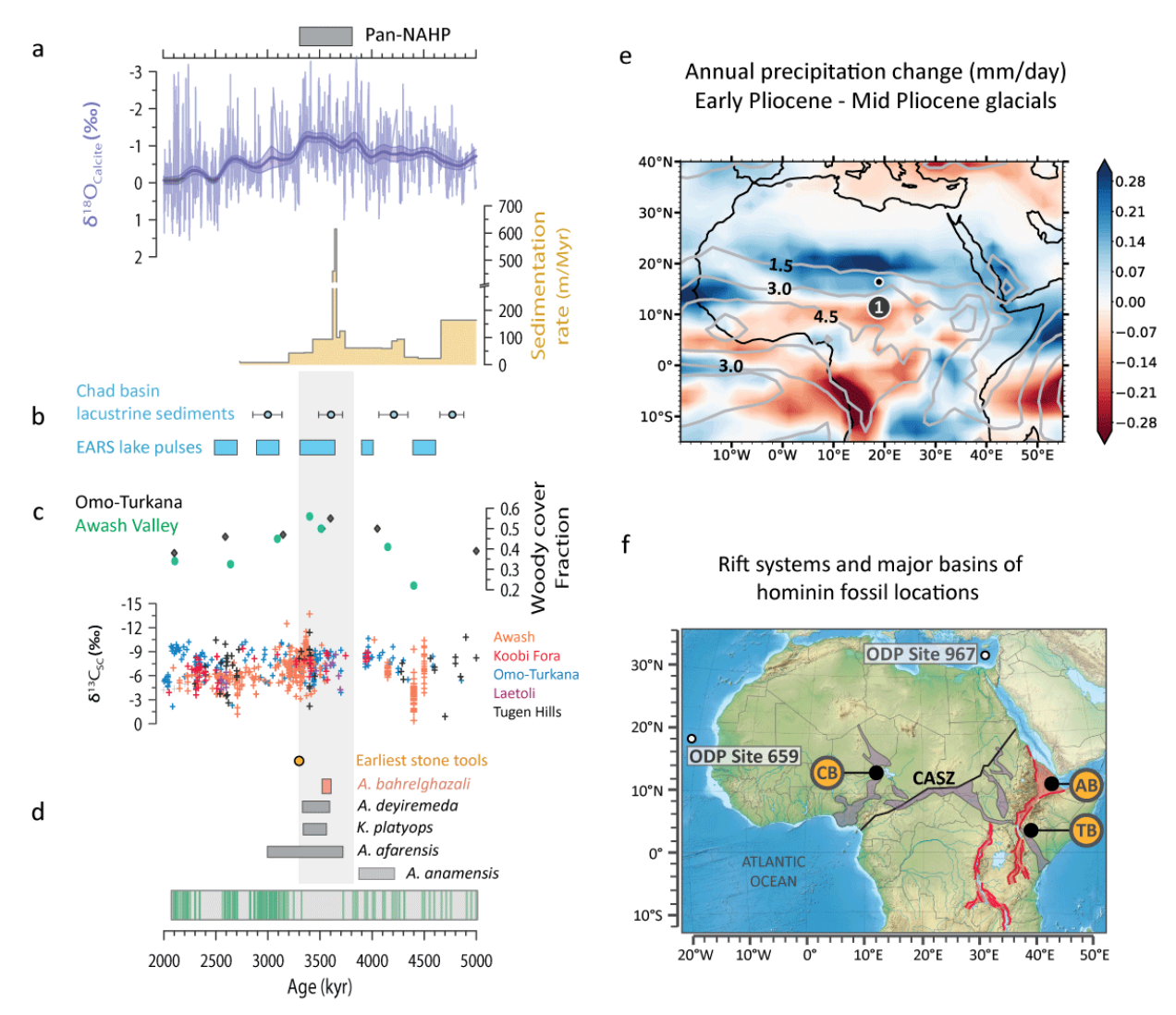


Figure 4| The Pan-NAHP and hominin evolution. a, ODP Site 967 stable oxygen isotope record for the 2-5 Myr period. b, Calculated Chad basin sedimentation rates<sup>38</sup>, with a significant increase within the Pan-NAHP. Occurrence of Chad basin lacustrine sediments and East African lake pulses over the Pliocene are shown<sup>32,33</sup>. c, Reconstructed woody cover fraction for Omo-Turkana Basin and Awash Valley (Afar Basin)<sup>36</sup> and soil carbonate  $\delta^{13}$ C values from wider east Africa<sup>37</sup>, with a minimum within the Pan-NAHP d, Estimated time spans for multiple hominin remains discovered within the Pan-NAHP (see Extended Data Fig. 8). The oldest known stone tools follow the Pan-NAHP termination<sup>48</sup>. Eastern Mediterranean sapropel stack is shown below. e, Climate model results with annual precipitation change from Early Pliocene to Mid-Pliocene glacials, indicating enhanced Early Pliocene North African precipitation. Circled numbers 1, 2 and 3 represent fossil discovery sites for A. bahrelgazali (Koro Toro, Chad Basin)<sup>9</sup>, and other East African australopithecines from Woranso-Mille, central Afar and Lake Turkana, Kenya<sup>44,45</sup> (see Extended Data Fig. 8). Contours indicate isohyets for Mid Pliocene glacial climate. f, Map with the East and Central African rift systems, which have been suggested as a possible migration path for East African hominins to the Chad Basin<sup>33</sup> (see Extended Data Fig. 8). Miocene-Holocene East African rift system and Early-Late Cretaceous Central African rift system are highlighted in red and purple, respectively<sup>33</sup>. ODP Sites 659 and 967 are indicated by white dots. CASZ, Central African shear zone (thick black line); CB, Chad Basin; AB, Afar Basin; TB, Turkana Basin.

372

373

374

375

376

377

378

379

380

381

382

383

384

385

386

387

388

# Methods

Eastern Mediterranean sapropel compilation

To generate the sapropel stack, we combine sapropel stratigraphies of all available deep eastern
Mediterranean Ocean Drilling Program (ODP) sites, recognized based on visual core
descriptions and colour reflectance data. These were subsequently tuned to NH boreal
insolation maxima and subsequently correlated with our ODP Site 967 stable oxygen isotope
record. All available ODP sediment records are located at >900 m water depths<sup>7,17</sup> (Extended
Data Fig.1).

397 Data Fig.1).398 At shallowe

At shallower than ~400 m depth in the eastern Mediterranean, sapropels are unlikely to be preserved due to sufficiently ventilated conditions<sup>14,16,51</sup>. Below this level, the organic matter quantity buried in sediment changes with water depth<sup>16,51</sup>, and is determined by a) the degradation rate during settling through the water column and b) the degradation rate at the sediment-water interface<sup>51</sup>. The organic matter import flux (amount of organic matter reaching the sediment-water interface at a certain depth) decreases with water depth<sup>16,51</sup>. However, burial efficiency during sapropel formation (amount of organic matter amount buried in sediment, after water column and sediment-water interface degradation) increases with water depth, due to decreasing oxidant fluxes at the sediment-water interface.

After burial, organic matter undergoes post-depositional oxidation in the modern, unstratified Mediterranean. Therefore, high organic carbon contents reported from sapropels are a consequence of both elevated productivity and enhanced preservation<sup>52</sup>. The abundance of microfossils has suggested that sapropel deposition dominantly resulted from increased productivity, due to the presence of a deep chlorophyll maximum (DCM) in the photic zone resulting from pycnocline shoaling forced by reduced buoyancy followed by elevated freshwater influx<sup>14,53</sup>. Furthermore, elevated Ba/Al ratios within sapropels have been attributed to barite (BaSO<sub>4</sub>) enrichment in sinking organic matter, linking to enhanced productivity<sup>14</sup>. Barite dissolution and Ba mobilization can alter the original sea floor Ba content, if sulfate reducing conditions occur<sup>54</sup>. However, Ba/Al has been established as an indicator of original sapropel extent where organic matter has been oxidized, as biogenic Ba flux preservation is the highest of all biogenic components<sup>54</sup> and has been applied to estimate Mediterranean paleoproductivity<sup>55</sup>. Alternatively, depleted bulk sediment N isotope values (δ<sup>15</sup>N) has been suggested to reflect enhanced preservation rather than elevated productivity, as oxidation would have released <sup>15</sup>N-enriched components to the sediment, elevating sedimentary

 $\delta^{15}N^{ref.56}$ . Similar depleted  $\delta^{15}N$  values to that of the most recent sapropel were recorded from modern Mediterranean sinking particulate matter, suggesting lower productivities during sapropel formation<sup>56</sup>. Sapropel preservation is mainly affected by the post-depositional oxygen availability. Post-depositional oxidation can partially or completely degrade organic carbon (sapropel burndown), resulting in the loss of dark appearance of sediments. The Ba/Al ratio is commonly used to identify burned down sapropels<sup>7,14</sup>. Modelling efforts have shown that the burndown rate is inversely proportional to the organic matter content of a sapropel<sup>57</sup>.

Intensification of eastern Mediterranean organic carbon burial over time can be observed at the four ODP sites, which increased substantially the sapropel preservation frequency. At ODP sites 967 and 969, preserved sapropels are absent for 3.2-5.3 Myr and 3.2-4.3 Myr, respectively, which indicates complete post-depositional oxidation. This observation is further supported by ODP 967 Ba/Al record. Before 3.2 Myr, nutrient supply to the eastern Mediterranean was likely substantially reduced<sup>7</sup>. Therefore, we suggest that low organic carbon fluxes to the deep basin were insufficient to generate preserved sapropels during these intervals. Occasional sapropel preservation can be observed at Site 969, before 4.3 Myr. At ODP Site 966, the sediment record is tectonically disturbed within the 5.3-4.5 Myr interval<sup>58</sup>. Between 4.5 and 3.8 Myr, Site 966 sapropel preservation is frequent, compared to Site 969<sup>17</sup>. We interpret this to be a result of the organic carbon import decrease to deeper water depths at Site 969, which was insufficient for organic carbon burial. Between 3.70 and 3.82 Myr, there are only two preserved sapropels at Site 966, with low (~1%) organic carbon contents. Therefore, preserved sapropels are absent across the entire eastern Mediterranean ODP cores within the 3.3-3.7 Myr period (while only two low-organic carbon sapropels are observed between 3.7 and 3.82 Myr, only at Site 966)<sup>7,17,58</sup>. We posit that organic matter imported to even the shallowest eastern Mediterranean site (Site 966 at ~940 m water depth) was insufficient for sapropel preservation during the 3.3-3.7 Myr period, which indicates even more reduced surface productivity compared to the Early Pliocene. Our hypothesis is further supported by ODP Site 967  $\delta^{18}$ O data, which reflects that the freshwater runoff was maximized during the 3.8-3.3 Myr period, compared to the rest of the Pliocene, which would have caused more intense stratification and bottom anoxia. The absence of sapropels during the period of maximum possible stratification and anoxia (that lead to higher preservation) suggests further reduced organic carbon flux (therefore, surface productivity) during the 3.8-3.3 Myr period.

422

423

424

425

426

427

428

429

430

431

432

433

434

435

436

437

438

439

440

441

442

443

444

445

446

447

448

449

450

451

# **Climate Model Experiments**

454

484

We observe a considerable mean global ice volume increase during the M2 glaciation and 455 subsequent Mid-Pliocene glacials, compared to the Early Pliocene. Pan-NAHP termination is 456 coeval with the M2 glaciation (~3.34-3.27 Myr), and eastern Mediterranean organic carbon 457 burial intensifies subsequently. We calculate mean ice volumes for Early Pliocene and Mid 458 Pliocene glacials using a published ice volume reconstruction<sup>19</sup> (Extended Data Table 1). Our 459 calculations indicate that NH ice volume increased significantly more, compared to the 460 Southern Hemisphere (SH), during the M2 glaciation. As explained in the text, we speculate 461 that the ice volume increase disrupted stable humid conditions during the Pan-NAHP (and 462 relatively humid conditions through the 5.3-3.3 Myr period). To evaluate the possible impact 463 of increasing ice volumes on North African climate, we employed a coupled climate model, as 464 465 described below. Model components. Model experiments were carried out using the coupled climate model 466 GFDL CM2.1, which consists of dynamic ocean, atmosphere, land and sea ice components<sup>59</sup>. 467 The ocean component is updated to incorporate Modular Ocean Model version 5.1.0 (MOM5), 468 using a resolution of 1° latitude x 1° longitude x 50 vertical levels, with latitudinal refinement 469 within  $\pm 30^{\circ}$  latitude down to 0.33° at the equator, as in ref.<sup>59</sup>. The ocean and sea ice horizontal 470 grid uses a tripolar configuration, consisting of a regular latitude-longitude grid from 85°S to 471 65°N, and a bipolar grid north of 65°N with poles over North America and Eurasia. The other 472 model components are the same as in GFDL CM2.1, namely the GFDL Atmosphere Model 2, 473 Land Model 2 and Sea Ice Simulator. The atmosphere resolution is 2° latitude x 2.5° longitude 474 x 24 levels, as in the original GFDL CM2.1. 475 **Boundary conditions.** In this study, we use three experimental configurations, representing (i) 476 the Early Pliocene (5.3-3.4 Ma), (ii) the M2 glaciation (~3.3 Ma) and (iii) Mid Pliocene glacials 477 (3.27-3.0 Ma). A summary of these configurations is shown in Extended Data Table 1. The 478 Early Pliocene simulation serves as a control experiment, where our intention is to compare 479 480 results from glacial simulations with the Early Pliocene reference simulation. **Early Pliocene simulation.** The early Pliocene simulation is set up using PRISM4 boundary 481 conditions, as used in the Pliocene Model Intercomparison Project 2 (PlioMIP2)<sup>60</sup>. The 482 palaeogeography, including topography and bathymetry, ice sheet extents, and vegetation types 483

are all set according to the PRISM4 protocol. Note, we do not use the PlioMIP3 boundary

conditions<sup>61</sup>, since the simulations were designed and implemented before the PlioMIP3 protocols became available.

The M2 glacial and Mid Pliocene glacial simulations use PRISM4 boundary conditions as a starting point, with modifications to the ice sheets to match the total ice volume from the compilation of ref.<sup>19</sup>. The chosen timeslices of published ice sheet reconstructions represent a physically realistic representation of a target ice volume, rather than an exact Pliocene ice sheet reconstruction. We note that a similar approach of reconstructing ice boundary conditions was used in the Pliocene modelling experiments of ref.<sup>62</sup>, where they used ice model reconstructions from different time periods to match their targeted ice volume for the Pliocene M2 scenario.

- **M2 glacial simulation.** For the M2 glacial simulation, NH and SH ice sheets were derived 495 from 12.5 kyr and 7.5 kyr timeslices of the ICE-7G\_NA reconstruction<sup>63</sup>, to match total ice 496 volumes calculated for each hemisphere (NH = 52.13 m, SH = 62.16 m).
- Mid Pliocene glacial simulation. For this case, we imposed NH ice sheets derived from the ice sheet reconstruction of ICE-7G\_NA using their 8 ka timeslice<sup>63</sup>, to achieve a total ice volume of 10.17 m sea level equivalent (SLE). For the SH, we used ref.<sup>64</sup>, with their RCP4.5 scenario at year 5000 to achieve a total ice volume of 55.32 m SLE.
- Land surface properties The topography and bathymetry for all three configurations are shown in Extended Data Fig.9. Since the vegetation types are prescribed as a boundary condition, we keep vegetation fixed in all three scenarios, except where the land surface type is specifically adjusted to become an ice sheet. The land-sea mask is adjusted to accommodate the larger ice sheets in the glacial simulations (especially M2), but these changes are limited only to the ice regions. We do not make far-field adjustments for sea level change, i.e. continental shelves remain unchanged outside of the polar ice sheet regions.

One limitation of this approach is that it does not permit vegetation feedbacks induced by the ice sheet and climate changes. As noted above, vegetation changes and/or dynamic feedbacks have been found to play an important role in previous Pliocene simulations<sup>23,24,65,66</sup>. Since the vegetation changes tend to force precipitation in the same direction as our ice sheet perturbation (i.e. drier for more glacial climates), we would expect the signal to be larger if vegetation changes were included in the model. However, our method has the benefit of allowing a simpler chain of causality: We can directly attribute the climate changes to the presence of larger ice sheets, whereas adding vegetation changes would make this causality harder to determine.

While vegetation feedbacks are beyond the scope of the modelling presented here, a possible way to extend the study would be to use the climate model outputs from all 3 scenarios to drive an offline vegetation model (e.g. BIOME4)<sup>67</sup>. The offline-generated vegetation outputs could then be used as boundary conditions to re-run the climate model simulations, to check for an amplification (or otherwise) of the precipitation and circulation changes we have found.

# Mixing across narrow ocean gateways

- In the pre-industrial simulation of GFDL CM2.1<sup>ref.59</sup>, the Black Sea, Red Sea and Mediterranean Sea use parameterised tracer mixing across the narrow straits that connect these seas to the rest of the ocean (Turkish Straits, Bab el-Mandeb Straits and Strait of Gibraltar). This mixing is implemented because those straits are too narrow for the ocean grid to resolve. (The ocean model requires a minimum strait width of two grid-cells, i.e. ~200 km width). For our Pliocene simulations, we retain this parameterised mixing connecting all 3 of these marginal seas to the world ocean (Black Sea, Red Sea and Mediterranean Sea). This ensures the closest agreement to the PRISM4 topography and consistency with the pre-industrial simulation, while enabling the water mass properties of these marginal seas to be connected to the world ocean.
- Initial conditions and spinup. Climate model runs were initiated using idealised ocean temperature and salinity initial conditions. Salinity was set to a uniform global value of 34.7 psu. Initial temperature was constructed using (i) surface sea surface temperature (SST) values from the PRISM4 dataset, (ii) a uniform deep ocean 6 °C value everywhere below 500 m depth, and (iii) linear interpolation between 0 and 500 m from the PRISM4 SST and deep ocean temperatures. The deep ocean value was chosen to be slightly warmer than the anticipated equilibrium to enable the start of deep ocean circulation that tends to initiate when the ocean is losing heat. Atmosphere and land components were initiated using a "cold start" condition. These components have a much lower heat capacity than the ocean, so they quickly reach quasiequilibrium and the long-term spinup depends largely on ocean evolution. All three simulations were spun up from idealised initial conditions for 2000 years, using CO<sub>2</sub> forcing demarcated in Extended Data Table 1. The analyses use the mean of the last 50 years of simulation to reduce the impact of short-term variability.

### **ODP Site 967 Nd isotopes**

To evaluate sediment provenance at ODP Site 967 over the past 5 Myr, we measured Nd isotope values of the clay fraction of selected bulk sediment samples. Samples were chosen for

consecutive sapropel-marl couplets covering the entire 0-5 Myr age range (Extended Data Fig.

549 6). Sample preparation was carried out at the Fenner School of Environment & Society,

Australian National University. The procedure involved clay separation to separate aeolian silt,

followed by ultrasonic leaching to remove non-detrital matter as outlined in ref. <sup>68</sup>.

To separate the clay fraction from bulk sediment, ~1.5-2.5 g of each sample was gently crushed with an agate mortar and pestle. Each crushed sample was treated with a 5% NaPO<sub>3</sub> solution in a 50 ml centrifuge tube, and then kept on a mixing wheel overnight to prevent clay flocculation. The next day, the samples were centrifuged at 1,000 rpm for 360 seconds to separate the clay and silt fractions. The supernatant was decanted into a separate vial and centrifuged at 4,000 rpm to recover the clay fraction. This procedure was repeated 4-5 times for the remaining bulk sediments to extract as much clay as possible from each sample.

Sequential leaching involved initially mixing the separated clay fraction with ~8 ml of H<sub>2</sub>O at room temperature to remove the water soluble fraction. Samples were then centrifuged at 4,000 rpm to remove the supernatant solution. All samples were subsequently treated with 0.5 M Mg(NO<sub>3</sub>)<sub>2</sub> solutions at room temperature (to remove the exchangeable fraction, i.e. cations adsorbed to mineral surfaces), 1 M CH<sub>3</sub>COONa at room temperature (to remove the acid-soluble fraction such as carbonate, with sonication at room temperature for 5 minutes, repeated 3 times), 0.1 M NH<sub>2</sub>OH\*HCl at 80 °C (to remove reducible fraction such as Fe and Mn oxides, with sonication at 80°C for 6 minutes, repeated 3 times), 15% H<sub>2</sub>O<sub>2</sub>-0.02 M HNO<sub>3</sub> at 80 °C (sonication at 80°C for 3 minutes, repeated 5 times) and 3.2 M CH<sub>3</sub>COONH<sub>4</sub> in 20% HNO<sub>3</sub> at room temperature (centrifuged at 4000 rpm for 10 minutes, repeated three times, to remove oxidisable fraction such as organic matter and sulphides), successively. Sequential leaching was supported by sonication following the procedure elaborated in ref.<sup>68</sup>.

Dried samples were analysed for Nd isotope values at the Mawson Analytical Spectrometry Services (MASS) at the University of Adelaide (UoA). Following grinding, complete HF sample dissolution, and column exchange chromatography to separate Nd from the sample matrix, Nd isotope analyses were carried out using an ISOTOPX Phoenix thermal ionisation mass spectrometer (TIMS). Nd concentrations in each sample, required to determine the amount of Nd loaded for column exchange chromatography, were analysed using an Agilent 8900x triple quad inductively coupled plasma mass spectrometer (QQQ-ICP-MS) at Adelaide Microscopy (UoA). All Nd isotope ratios were normalized to the JNdi-1 standard (143 Nd/144 Nd = 0.512115 ± 0.000007), with independent measurements of JNdi-1 = 0.512121 ± 0.000006

(2σ, n=2). Isotopic signatures are expressed in epsilon notation, relative to the chondritic uniform reservoir value of 0.512638.

#### **Mediterranean box model experiments**

To estimate the freshwater input magnitude capable of generating a minimum shift of  $\sim$ 0.45% in ODP Site 967  $\delta^{18}$ O<sub>calcite</sub> to more negative long-term  $^{18}$ O<sub>calcite</sub> values, a Mediterranean Winter-Summer-Monsoon box model was employed (Extended Data Fig.2). The box model employed here is based on a family of models developed in refs. $^{15,25,69}$ . The box model is coupled to an exchange transport model with the Atlantic via the Strait of Gibraltar and consists of a winter mixed-layer box, which is subsequently split into a summer-mixed box and a summer-subthermocline box. For two months in late summer a surface layer monsoon box is included into which monsoon freshwater runoff is added. At the end of summer, the summer-mixed, summer-subthermocline, and monsoon boxes are homogenized to form a new winter mixed box. This annual cycle can then be repeated until the model reaches equilibrium under a given fixed forcing scenario.

The Mediterranean box model in ref. <sup>15</sup> employed a  $\delta^{18}O_{calcite}$  forward modelling strategy to estimate relative sea level at Gibraltar (RSL<sub>Gib</sub>). In our version of the model, RSL<sub>Gib</sub> is a forcing parameter, which was estimated from the global mean eustatic sea-level (ESL) record of ref. <sup>19</sup> based on the RSL<sub>Gib</sub> to ESL conversion of ref. <sup>15</sup>. Thus, if the key properties of the model boxes, such as temperature, salinity, and  $\delta^{18}O_{calcite}$ , are fixed while RSL<sub>Gib</sub> is allowed to change, the mean Mediterranean  $\delta^{18}O_{calcite}$  change solely due to RSL<sub>Gib</sub> changes can be separated from the initial  $\delta^{18}O_{calcite}$  record. This enables the model to be used in a sensitivity analysis to differentiate potential underlying causes of large-scale changes in ODP Site 967  $\delta^{18}O_{calcite}$ .

Mediterranean surface freshening during times of sapropel formation lead to negative  $\delta^{18}O_{calcite}$  anomalies due to both 1) isotopically depleted monsoon waters and 2) temperature concentration due to freshwater layer heating  $^{70}$ . It is not possible to determine the contribution from monsoon waters alone, without temperature measurements from surface-dwelling foraminifera  $^{70}$ . Therefore, to estimate the possible range of freshwater runoff and temperature concentration that would have generated the  $\sim 0.45\%$  shift, we estimate 3 parameters:

$$\Delta \delta^{18} O_{SST} = \frac{\partial \delta^{18} O_{Calcite}}{\partial SST}, \tag{1}$$

where  $\Delta \delta^{18} O_{SST}$  is the  $\delta^{18} O_{calcite}$  change per 1°C of mean annual sea surface temperature change, at a given RSL<sub>Gib</sub>, and

$$\Delta \delta^{18} O_{T_C} = \frac{\partial \delta^{18} O_{Calcite}}{\partial T_C}, \tag{2}$$

- where  $\Delta \delta^{18} O_{T_C}$  is the  $\delta^{18} O_{calcite}$  change per 1°C of surface layer temperature concentration, at
- a given RSL<sub>Gib</sub>, and

$$\Delta \delta^{18} O_{FWF} = \frac{\partial \delta^{18} O_{Calcite}}{\partial \Delta R}, \tag{3}$$

- where  $\Delta \delta^{18} O_{FWF}$  is the  $\delta^{18} O_{calcite}$  change for a freshwater runoff increment equivalent to pre-
- 616 Aswan Nile runoff at a given RSL<sub>Gib</sub> (Extended Data Fig. 2).
- We observe that in existing SST records<sup>42,71,72</sup> (only the record from Pissouri section, Cyprus
- goes back to 4 Myr), a rise in SST that can explain the  $\delta^{18}$ O<sub>calcite</sub> drop around 3.9-3.8 Myr does
- not exist (Extended Data Fig. 2b). Therefore, a large rise in SST can be excluded. Sensitivity
- studies on the temperature concentration effect during the deposition of Sapropel 5 (S5, 128-
- 621 122 kyr) suggests that the surface warming for a runoff increase by two times that of pre-Aswan
- Nile runoff may have resulted in an extra warming of the upper summer mixed layer of  $\sim 1.2$
- °C. Our sensitivity test indicates that a 1.2 °C can result in a  $\delta^{18}$ O<sub>calcite</sub> drop of only 0.24 %,
- which is less than the minimum of 0.45 %  $\delta^{18}$ O<sub>calcite</sub> drop we observe around 3.8 Myr. This
- suggests that at least 0.21 %  $\delta^{18}$ O<sub>calcite</sub> drop should be explained by an increase in runoff, which
- 626 is equivalent to 75% pre-Aswan runoff.

627

#### Statistical analysis of palaeoclimate proxy records

We have employed two well-established geochemical ratios for Northwest Africa and the 628 eastern Mediterranean, to assess the hydroclimate variability over the Plio-Pleistocene. For 629 west African ODP Site 659, aeolian material is mainly transported from the Sahel and the 630 Sahara, via the Saharan Air Layer<sup>10,73</sup>. Additional minor components are derived from 631 northward regions around Morocco, which are then delivered via Trade winds<sup>74</sup>. The major 632 fluvial material contributor is the Senegal River suspension, which brings weathered lateritic 633 soils formed under tropical conditions<sup>10,73</sup>. The [Al+Fe]/[Si+K+Ti] ratio has been established 634 as a traditional indicator of relative input of chemically weathered material under humid 635 conditions (Al and Fe rich) versus Si-rich Saharan dust<sup>10,73</sup>, providing a superior record of short 636 and long-term hydroclimate variability over Northwest Africa<sup>10</sup>. 637

- For the eastern Mediterranean ODP site 967, the Ti/Al ratio is well-established over several 638 studies as a reliable indicator of relative aeolian versus fluvial transport of terrigenous material 639 from North Africa<sup>7,75</sup>. Aeolian material (Ti-rich) is mainly derived from hyperarid regions of 640 northeastern Sahara via low-level winds. Fluvial component (Al-rich) from North Africa is 641 transported via the White Nile (from Sudd swamps) and the Blue Nile (from Ethiopian 642 Highlands), which later combines as the Main Nile<sup>27,76,77</sup>. While the Si content in Saharan dust 643 is enriched, the K/Al ratio in eastern Mediterranean sediments has been determined to reflect 644 the K-rich illite supply from the Northern Mediterranean borderlands, via Southeast European 645 rivers<sup>27,76,77</sup>, preventing the addition of K content to geochemical ratios as an indicator of North 646 African hydroclimate in eastern Mediterranean sediments. 647
- We further employ statistical methods to assess critical transitions in North African hydroclimate variability. To detect regime shifts in ODP Sites 967 and 659 geochemical and stable oxygen isotope records<sup>7,10</sup>, change points were estimated using the MATLAB built-in function 'findchangepts', following ref.<sup>7</sup>. Change-points were determined based on ice volume mean and standard deviation; a maximum of three change-points was stipulated as a parsimonious balance between constraining outputs to the most significant changes while allowing a >1 outcome.

#### Data availability

- The authors declare that all the data supporting the findings of this study are available with the
- 657 manuscript, uploaded as additional files.

#### 658 References

- 1. Shanahan, T. M. et al. The time-transgressive termination of the African Humid Period. Nat.
- 660 *Geosci.* **8**, 140–144 (2015).
- 2. Skonieczny, C. et al. African humid periods triggered the reactivation of a large river system in
- Western Sahara. *Nat. Commun.* **6**, 8751 (2015).
- 3. Osborne, A. H. et al. A humid corridor across the Sahara for the migration of early modern
- humans out of Africa 120,000 years ago. *Proc. Natl. Acad. Sci.* **105**, 16444–16447 (2008).
- 4. Larrasoaña, J. C., Roberts, A. P. & Rohling, E. J. Dynamics of Green Sahara Periods and Their
- Role in Hominin Evolution. *PLoS ONE* **8**, e76514 (2013).

- 5. Kuper, R. & Kröpelin, S. Climate-Controlled Holocene Occupation in the Sahara: Motor of
- Africa's Evolution. *Science* **313**, 803–807 (2006).
- 669 6. Kröpelin, S. et al. Climate-Driven Ecosystem Succession in the Sahara: The Past 6000 Years.
- 670 *Science* **320**, 765–768 (2008).
- 7. Grant, K. M. et al. Organic carbon burial in Mediterranean sapropels intensified during Green
- Sahara Periods since 3.2 Myr ago. *Commun. Earth Environ.* **3**, 11 (2022).
- 8. Amarathunga, U. et al. Sill-controlled salinity contrasts followed post-Messinian flooding of the
- 674 Mediterranean. *Nat. Geosci.* **15**, 720–725 (2022).
- 9. Brunet, M. et al. The first australopithecine 2,500 kilometres west of the Rift Valley (Chad).
- 676 *Nature* **378**, 273–275 (1995).
- 10. Crocker, A. J. et al. Astronomically controlled aridity in the Sahara since at least 11 million years
- 678 ago. *Nat. Geosci.* **15**, 671–676 (2022).
- 11. Menviel, L. et al. Drivers of the evolution and amplitude of African Humid Periods. Commun.
- *Earth Environ.* **2**, 237 (2021).
- 681 12. deMenocal, P. et al. Abrupt onset and termination of the African Humid Period: rapid climate
- responses to gradual insolation forcing. *Quat. Sci. Rev.* **19**, 347–361 (2000).
- 683 13. Rossignol-Strick, M. African monsoons, an immediate climate response to orbital insolation.
- 684 *Nature* **304**, 46–49 (1983).
- 14. Rohling, E. J., Marino, G. & Grant, K. M. Mediterranean climate and oceanography, and the
- periodic development of anoxic events (sapropels). Earth-Sci. Rev. 143, 62–97 (2015).
- 15. Rohling, E. J. *et al.* Sea-level and deep-sea-temperature variability over the past 5.3 million years.
- 688 *Nature* **508**, 477–482 (2014).
- 689 16. De Lange, G. J. et al. Synchronous basin-wide formation and redox-controlled preservation of a
- 690 Mediterranean sapropel. *Nat. Geosci.* **1**, 606–610 (2008).
- 691 17. Emeis, K.-C., Sakamoto, T., Wehausen, R. & Brumsack, H.-J. The sapropel record of the eastern
- Mediterranean Sea results of Ocean Drilling Program Leg 160. *Palaeogeogr. Palaeoclimatol.*
- 693 *Palaeoecol.* **158**, 371–395 (2000).

- 18. Garcin, Y. et al. Short-lived increase in erosion during the African Humid Period: Evidence from
- the northern Kenya Rift. Earth Planet. Sci. Lett. 459, 58–69 (2017).
- 696 19. Rohling, E. J. et al. Sea level and deep-sea temperature reconstructions suggest quasi-stable states
- and critical transitions over the past 40 million years. Sci. Adv. 7, eabf5326 (2021).
- 698 20. Routson, C. C. et al. Mid-latitude net precipitation decreased with Arctic warming during the
- 699 Holocene. *Nature* **568**, 83–87 (2019).
- 700 21. Chiang, J. C. H. & Friedman, A. R. Extratropical Cooling, Interhemispheric Thermal Gradients,
- and Tropical Climate Change. Annu. Rev. Earth Planet. Sci. 40, 383–412 (2012).
- 702 22. Schneider, T., Bischoff, T. & Haug, G. H. Migrations and dynamics of the intertropical
- 703 convergence zone. *Nature* **513**, 45–53 (2014).
- 704 23. Stepanek, C., Samakinwa, E., Knorr, G. & Lohmann, G. Contribution of the coupled atmosphere–
- ocean–sea ice–vegetation model COSMOS to the PlioMIP2. Clim. Past 16, 2275–2323 (2020).
- 706 24. Willeit, M., Ganopolski, A. & Feulner, G. On the effect of orbital forcing on mid-Pliocene
- climate, vegetation and ice sheets. Clim. Past 9, 1749–1759 (2013).
- 708 25. Heslop, D., Amarathunga, U. & Rohling, E. J. Estimating Plio-Pleistocene North African
- 709 monsoon runoff into the Mediterranean Sea and temperature impacts. *Paleoceanogr*.
- 710 *Paleoclimatology* **38**, e2023PA004677 (2023).
- 711 26. Laskar, J., Fienga, A., Gastineau, M. & Manche, H. La2010: a new orbital solution for the long-
- term motion of the Earth. Astron. Astrophys. **532**, A89 (2011).
- 713 27. Beuscher, S. et al. End-member modelling as a tool for climate reconstruction—An Eastern
- 714 Mediterranean case study. *PLOS ONE* **12**, e0185136 (2017).
- 715 28. Garzanti, E., Andò, S., Padoan, M., Vezzoli, G. & El Kammar, A. The modern Nile sediment
- 716 system: Processes and products. *Quat. Sci. Rev.* **130**, 9–56 (2015).
- 717 29. Bastian, L. et al. Co-variations of climate and silicate weathering in the Nile Basin during the
- 718 Late Pleistocene. *Quat. Sci. Rev.* **264**, 107012 (2021).
- 30. Scheuvens, D., Schütz, L., Kandler, K., Ebert, M. & Weinbruch, S. Bulk composition of northern
- African dust and its source sediments A compilation. *Earth-Sci. Rev.* **116**, 170–194 (2013).

- 721 31. Jewell, A. M. et al. Three North African dust source areas and their geochemical fingerprint.
- 722 Earth Planet. Sci. Lett. **554**, 116645 (2021).
- 723 32. Trauth, M. H., Maslin, M. A., Deino, A. & Strecker, M. R. Late Cenozoic Moisture History of
- 724 East Africa. *Science* **309**, 2051–2053 (2005).
- 725 33. Maslin, M. A. et al. East African climate pulses and early human evolution. Quat. Sci. Rev. 101,
- 726 1–17 (2014).
- 34. Joordens, J. C. A., Feibel, C. S., Vonhof, H. B., Schulp, A. S. & Kroon, D. Relevance of the
- eastern African coastal forest for early hominin biogeography. J. Hum. Evol. 131, 176–202
- 729 (2019).
- 730 35. Hernández Fernández, M. & Vrba, E. S. Plio-Pleistocene climatic change in the Turkana Basin
- 731 (East Africa): Evidence from large mammal faunas. J. Hum. Evol. 50, 595–626 (2006).
- 732 36. Cerling, T. E. et al. Woody cover and hominin environments in the past 6 million years. *Nature*
- **476**, 51–56 (2011).
- 734 37. Levin, N. E. Environment and Climate of Early Human Evolution. Annu. Rev. Earth Planet. Sci.
- **43**, 405–429 (2015).
- 736 38. Lebatard, A.-E. *et al.* Application of the authigenic 10Be/9Be dating method to continental
- 737 sediments: Reconstruction of the Mio-Pleistocene sedimentary sequence in the early hominid
- fossiliferous areas of the northern Chad Basin. Earth Planet. Sci. Lett. 297, 57–70 (2010).
- 739 39. Moussa, A. et al. Lake Chad sedimentation and environments during the late Miocene and
- Pliocene: New evidence from mineralogy and chemistry of the Bol core sediments. J. Afr. Earth
- 741 *Sci.* **118**, 192–204 (2016).
- 742 40. Brierley, C. M. et al. Greatly Expanded Tropical Warm Pool and Weakened Hadley Circulation
- 743 in the Early Pliocene. *Science* **323**, 1714–1718 (2009).
- 41. Herbert, T. D., Peterson, L. C., Lawrence, K. T. & Liu, Z. Tropical Ocean Temperatures Over the
- Past 3.5 Million Years. *Science* **328**, 1530–1534 (2010).
- 42. Herbert, T. D. et al. Late Miocene global cooling and the rise of modern ecosystems. *Nat. Geosci.*
- **9**, 843–847 (2016).

- 748 43. Park, J.-Y., Bader, J. & Matei, D. Northern-hemispheric differential warming is the key to
- understanding the discrepancies in the projected Sahel rainfall. *Nat. Commun.* **6**, 5985 (2015).
- 750 44. Haile-Selassie, Y. et al. New species from Ethiopia further expands Middle Pliocene hominin
- 751 diversity. *Nature* **521**, 483–488 (2015).
- 45. Wood, B. & K. Boyle, E. Hominin taxic diversity: Fact or fantasy?: Hominin taxic diversity. Am.
- 753 *J. Phys. Anthropol.* **159**, 37–78 (2016).
- 46. Guy, F. et al. Symphyseal shape variation in extant and fossil hominoids, and the symphysis of
- Australopithecus bahrelghazali. *J. Hum. Evol.* **55**, 37–47 (2008).
- 47. Maxwell, S. J., Hopley, P. J., Upchurch, P. & Soligo, C. Sporadic sampling, not climatic forcing,
- drives observed early hominin diversity. *Proc. Natl. Acad. Sci.* **115**, 4891–4896 (2018).
- 48. Harmand, S. *et al.* 3.3-million-year-old stone tools from Lomekwi 3, West Turkana, Kenya.
- 759 *Nature* **521**, 310–315 (2015).
- 49. Zeller, E. et al. Human adaptation to diverse biomes over the past 3 million years. Science 380,
- 761 604–608 (2023).
- 50. Cuthbert, M. O. et al. Modelling the role of groundwater hydro-refugia in East African hominin
- 763 evolution and dispersal. *Nat. Commun.* **8**, 15696 (2017).
- 764 51. Murat, A. & Got, H. Organic carbon variations of the eastern Mediterranean Holocene sapropel: a
- key for understanding formation processes. *Palaeogeogr. Palaeoclimatol. Palaeoecol.* **158**, 241–
- 766 257 (2000).
- 52. Nijenhuis, I. A. & De Lange, Gert. J. Geochemical constraints on Pliocene sapropel formation in
- 768 the eastern Mediterranean. *Mar. Geol.* **163**, 41–63 (2000).
- 53. Castradori, D. Calcareous nannofossils and the origin of eastern Mediterranean sapropels.
- 770 *Paleoceanography* **8**, 459–471 (1993).
- 54. Dymond, J., Suess, E. & Lyle, M. Barium in deep-sea sediment: a geochemical proxy for
- paleoproductivity. *Paleoceanography* 7, 163–181 (1992).
- 55. Van Os, B. J. H., Lourens, L. J., Hilgen, F. J., De Lange, G. J. & Beaufort, L. The formation of
- Pliocene sapropels and carbonate cycles in the Mediterranean: Diagenesis, dilution, and
- 775 productivity. *Paleoceanography* **9**, 601–617 (1994).

- 56. Möbius, J., Lahajnar, N. & Emeis, K.-C. Diagenetic control of nitrogen isotope ratios in Holocene
- sapropels and recent sediments from the Eastern Mediterranean Sea. *Biogeosciences* 7, 3901–
- 778 3914 (2010).
- 57. Jung, M., Ilmberger, J., Mangini, A. & Emeis, K.-C. Why some Mediterranean sapropels
- survived burn-down (and others did not). *Mar. Geol.* **141**, 51–60 (1997).
- 781 58. Emeis, K.-C., Robertson, A. H. & Richter, C. Site 966, Initial Reports. *Proc. Ocean Drill*.
- 782 *Program* **160**, (1996).
- 783 59. Delworth, T. L. et al. GFDL's CM2 Global Coupled Climate Models. Part I: Formulation and
- 784 Simulation Characteristics. *J. Clim.* **19**, 643–674 (2006).
- 785 60. Haywood, A. M. et al. The Pliocene Model Intercomparison Project (PlioMIP) Phase 2: scientific
- objectives and experimental design. *Clim. Past* **12**, 663–675 (2016).
- 787 61. Haywood, A. M. et al. Pliocene Model Intercomparison Project Phase 3 (PlioMIP3) Science
- plan and experimental design. Glob. Planet. Change 232, 104316 (2024).
- 789 62. Dolan, A. M. et al. Modelling the enigmatic Late Pliocene Glacial Event Marine Isotope Stage
- 790 M2. Glob. Planet. Change **128**, 47–60 (2015).
- 791 63. Roy, K. & Peltier, W. R. Relative sea level in the Western Mediterranean basin: A regional test of
- 792 the ICE-7G NA (VM7) model and a constraint on late Holocene Antarctic deglaciation. Quat.
- 793 *Sci. Rev.* **183**, 76–87 (2018).
- 794 64. Golledge, N. R. et al. The multi-millennial Antarctic commitment to future sea-level rise. Nature
- **526**, 421–425 (2015).
- 796 65. Feng, R. et al. Past terrestrial hydroclimate sensitivity controlled by Earth system feedbacks. Nat.
- 797 *Commun.* **13**, 1306 (2022).
- 798 66. Prescott, C. L., Dolan, A. M., Haywood, A. M., Hunter, S. J. & Tindall, J. C. Regional climate
- and vegetation response to orbital forcing within the mid-Pliocene Warm Period: A study using
- 800 HadCM3. Glob. Planet. Change 161, 231–243 (2018).
- 801 67. Salzmann, U., Haywood, A. M., Lunt, D. J., Valdes, P. J. & Hill, D. J. A new global biome
- reconstruction and data-model comparison for the Middle Pliocene. *Glob. Ecol. Biogeogr.* 17,
- 803 432–447 (2008).

- 804 68. Francke, A., Carney, S., Wilcox, P. & Dosseto, A. Sample preparation for determination of
- comminution ages in lacustrine and marine sediments. *Chem. Geol.* **479**, 123–135 (2018).
- 806 69. Rohling, E. J. et al. Reconstructing past planktic foraminiferal habitats using stable isotope data: a
- case history for Mediterranean sapropel S5. *Mar. Micropaleontol.* **50**, 89–123 (2004).
- 808 70. Amies, J. D., Rohling, E. J., Grant, K. M., Rodríguez-Sanz, L. & Marino, G. Quantification of
- African Monsoon Runoff During Last Interglacial Sapropel S5. *Paleoceanogr. Paleoclimatology*
- **34**, 1487–1516 (2019).
- 71. Athanasiou, M. et al. Sea surface temperatures and environmental conditions during the "warm
- Pliocene" interval (~ 4.1–3.2 Ma) in the Eastern Mediterranean (Cyprus). *Glob. Planet. Change*
- **150**, 46–57 (2017).
- 72. Khélifi, N., Sarnthein, M., Frank, M., Andersen, N. & Garbe-Schönberg, D. Late Pliocene
- variations of the Mediterranean outflow. *Mar. Geol.* **357**, 182–194 (2014).
- 73. Mulitza, S. et al. Increase in African dust flux at the onset of commercial agriculture in the Sahel
- 817 region. *Nature* **466**, 226–228 (2010).
- 818 74. O'Mara, N. A. et al. Pleistocene drivers of Northwest African hydroclimate and vegetation. Nat.
- 819 *Commun.* **13**, 3552 (2022).
- 820 75. Larrasoaña, J. C., Roberts, A. P., Rohling, E. J., Winklhofer, M. & Wehausen, R. Three million
- years of monsoon variability over the northern Sahara. Clim. Dyn. 21, 689–698 (2003).
- 76. Wu, J., Böning, P., Pahnke, K., Tachikawa, K. & De Lange, G. J. Unraveling North-African
- riverine and eolian contributions to central Mediterranean sediments during Holocene sapropel S1
- 824 formation. Quat. Sci. Rev. 152, 31–48 (2016).
- 825 77. Wu, J., Filippidi, A., Davies, G. R. & De Lange, G. J. Riverine supply to the eastern
- Mediterranean during last interglacial sapropel S5 formation: A basin-wide perspective. *Chem.*
- 827 *Geol.* **485**, 74–89 (2018).
- 828 78. Schlitzer, Reiner, Ocean Data View, https://odv.awi.de, 2023.
- 829 79. Fairhead, J. D. The Mesozoic West and Central Africa Rift System (WCARS) and the older
- 830 Kandi Shear Zone (KSZ): Rifting and tectonics of North Africa and South America and fragmentation
- of Gondwana based on geophysical investigations. J. Afr. Earth Sci. 199, 104817 (2023).

- 832 80. Makeen, Y. M. et al. Sedimentology, petrography, and reservoir quality of the Zarga and
- 633 Ghazal formations in the Keyi oilfield, Muglad Basin, Sudan. Sci. Rep. 11, 743 (2021).
- 81. Macgregor, D. History of the development of the East African Rift System: A series of
- interpreted maps through time. J. Afr. Earth Sci. 101, 232–252 (2015).

837

- Materials & Correspondence should be addressed to U.A. (udara.amar@princeton.edu)
- 838 Acknowledgements
- 839 This work contributes to Australian Research Council projects FL120100050 and
- 840 DP2000101157 (EJR), DE190100042 (KMG), DP190100874 (APR, DH), DE220100279
- 841 (DKH) and the Australia-New Zealand IODP Consortium (ANZIC) Legacy/Special Analytical
- Funding grant LE160100067 (KMG). We thank Mawson Analytical Spectrometry Services,
- University of Adelaide for contributing to Nd isotope measurements.

#### 844 Author contributions

- U.A. designed and led the study, prepared samples for Nd isotope analyses, analyzed the data
- and climate model outputs, developed the hypothesis, generated the figures and wrote the
- paper; A.F. advised on Nd isotope analysis and data interpretation; R.M.K carried out Nd
- isotope analyses; D.K.H. generated the climate model ice sheet configurations and performed
- modelling experiments; D.H. advised on statistical analyses and performed the box model
- experiments; K.M.G. and J.L. helped with sample selection and preparation; E.J.R. advised on
- data interpretation; all authors contributed to manuscript development.

# **Competing interests**

853 The authors declare no competing interests.

854